This article has been accepted for publication in a future issue of this journal, but has not been fully edited. Content may change prior to final publication. Citation information: DOI 10.1109/JESTPE.2018.2878925, IEEE Journal of Emerging and Selected Topics in Power Electronics

A Family of Switched-Resonant Converters with Wide Conversion Ratio and Controlled Sourcing Features for Volume-Sensitive Applications

Alon Cervera, *Student Member, IEEE* and Mor Mordechai Peretz, *Member, IEEE*
The Center for Power Electronics and Mixed-Signal IC, Department of Electrical and Computer Engineering
Ben-Gurion University of the Negev, P.O. Box 653, Beer-Sheva, 8410501 Israel
cervera@bgu.ac.il, morp@ee.bgu.ac.il
http://www.ee.bgu.ac.il/~pemic

***Abstract*— In this study, a family of switched-resonant converters with high efficiency over a wide conversion ratio range is introduced. Inspired by the gyrator resonant switched-capacitor concept, the new topology provides high efficiency over wide and continuous range of conversion ratios using a single resonator. This is enabled by new modes of operation (switching sequences) developed and analyzed in this study, that modify the charge-balance of the flying capacitor. By that, the sourcing as well as the efficiency characteristics of the converter can be shaped to peak at various conversion ratios. A generalized methodology is presented to describe resonant converters with multiple operation-modes as two-port which is then used to analyze several operational modes of the presented topology. Experimental results validate the developed theoretical model and demonstrate the superiority of the concept in terms of efficiency (over 10%) and current-sourcing capabilities (over 80%) using a compact 5W prototype.**

Keywords*— switch-mode converters; switched-capacitor converter; gyrator; efficiency; switched-resonant converters

I. Introduction

Switched-capacitor converters (SCCs) present superior power density compared to switched-inductor converters. In a variety of applications where the volume of the power management portion is critical such as portable and mobile electronics, SCCs are already being utilized as a preliminary conversion stage. A primary limitation that prevents the technology to replace inductor-based converters is the limited voltage regulation capability which stems from the tight relationship between the voltage gain and the converter efficiency [1-10]. In [1] it has been demonstrated that for any switch and multi-tank configuration, the efficiency is linearly tied to the output current. In [6] it is then emphasized that for voltage regulation the efficiency is linearly proportional to the ratio between the output voltage and target one (the no load SCC output voltage, V_{out} / V_{target}). Several models have been developed to describe and explore the performance of SCCs [3-5], later extended to state-space analysis [7] and average-current modelling [9]; model comparison has been carried out by [10].

Regulation can be achieved either by varying the SCC switching frequency/duty [1,11,12], or by inserting a post regulation stage [13-15] to match the required conversion ratio. Another possible approach for voltage regulation by SCC is to generate multiple target voltages using multiple flying-capacitor cells and therefore increase the effective operation range [1,16-20]; the system efficiency however, would remain of a discrete nature.

Reduced switching losses allow higher operating frequency and reduced volume, which motivated various derivatives of resonant-type SCC (RSCC) to be employed [21-31]: Step-up/down/inverting topologies have been presented in [21-23], later extended to multilevel high step-down converters [24-26]. Specific step-up application for thermoelectric power generation has been presented in [27-29], and design for chip-integration in [30-31]. By introducing GaN technology, recent publications have obtained unprecedented power densities of 500-2200 W/in^3 for fixed conversion ratios [32,33]. Since the operation of RSCCs is similar to the conventional SCCs in a sense that similar switching sequences are applied, the efficiency of the converter is still associated with the voltage gain. As a result, the challenge of regulating the output remains, i.e. to produce an output voltage that is different than the natural open-loop target voltage still requires post-regulation [1,33-35]. The reason for that is when the output voltage is different from the target voltage, the charge-balance of the flying capacitor(s) is not satisfied [9,36,37], affecting the average current. In such case, the converter's operating point shifts to the point where the voltage drop across the parasitic series resistances matches the difference between the output and target voltages.

More sophisticated approaches to facilitate voltage regulation without losses introduce an additional charge/discharge path, i.e. additional switching state or states to satisfy the capacitor charge-balance. This has been adopted in several previous studies by either internally circulating residual charge [38], by hybrid operation above resonant frequency to exhibit inductive behavior (partially losing soft-switching capabilities) [39-43], or by combining resonant and linear operation to completely deplete the residual charge in every switching cycle [44-45].

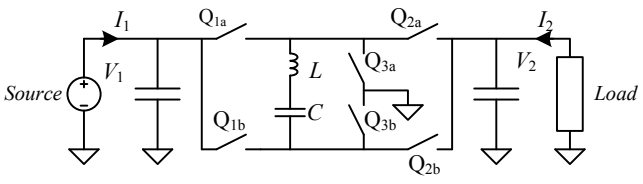

Fig. 1 The presented multi-mode switched-resonant converter.

A recently-developed gyrator mode resonant switched-capacitor converter (GRSCC) presented in [36,46-48] has demonstrated a unique potential for efficient voltage regulation over a wide range of conversion ratios. The main attribute of the GRSCC is that it disengages the efficiency of the system from the voltage gain. This is achieved by introducing an additional switching state to balance the mismatch between the input and the output average currents. As a result, the conventional SCC topology is transformed to a voltage-dependent current source, i.e. a gyrator-like converter [49-52]. The GRSCC exhibits

This article has been accepted for publication in a future issue of this journal, but has not been fully edited. Content may change prior to final publication. Citation information: DOI 10.1109/JESTPE.2018.2878925, IEEE Journal of Emerging and Selected Topics in Power Electronics

continuous gain that can be controlled by pulse-density modulation (PDM) [53,54]. Nevertheless, high conversion ratios in this topology remain problematic due to the large mismatch between the input and output current, which translates into a high circulating current within the charge-balancing state. This is overcome in the presented family of switched-resonant converters (SwRCs), by introducing additional switching states. This new method of operation enables disengagement of the system's efficiency from the voltage gain. A feature resided thus far in switched-inductor converters. Nonetheless, since these converters share a similar hardware configuration with their precursors, they still retain the volume benefits.

The objective of this study is to introduce a new SwRC with enhanced current sourcing or sinking capabilities, high-efficiency over a wide range of conversion ratios, and present a unique methodology to shape the efficiency characteristics of the converter by the switching scheme. The primary advantage of the SwRC family is that wide and continuous conversion ratio with high efficiency is achieved using a single energy transfer cell (i.e., one flying capacitor). This allows ultimate volume and complexity reduction when compared to other multi-target voltage converters that employ switched-capacitor [16-18] or switched-resonant approaches [20,55,56]. A further objective of this research is to develop a generalized methodology to describe the input-output characteristics of resonant converters with multiple operation-modes as two-port networks. A variety of ten operation modes (switching schemes of the converter) out of the presented family are demonstrated as a showcase of power-sourcing and efficiency capabilities of the new converter.

The SwRC family in its simplistic form, shown in Fig. 1, is a modification of a soft-switched resonant SCC with switch assembly inspired by multi-target voltage converters such as the binary/Fibonacci SCC [17,20] or the GTSP [16,18]. As opposed to other configurations that employ multiple flying tanks, in this study a single energy-transfer cell is used. The switches configuration allows the resonator to connect the input or the output ports directly or with reverse polarity, as well as a series-parallel connection to either port. By that, multiple switching possibilities to achieve charge balance of the tank can be realized. As demonstrated previously in [36,44-46], this is an enabler to disengage the rigid relationship between the efficiency and the voltage gain.

The rest of the paper is organized as follows: Section II provides a general analysis for a series LC switched-resonant converter as a two-port network and derives an expression for the converter's efficiency represented by the network impedances. Section III delineates ten operation modes of the new family along with analysis and comparison of performance for the various modes. Experimental results are provided in Section IV. Section V concludes the paper.

II. Generalized Conversion Characteristics of a Switched-Resonator Network as a Two-Port

A switch-mode converter can be described as a two-port network, as illustrated in Fig. 2, using average and dynamic behavioral modeling [44,46] to define a relationship between the input and output port voltages V_1, V_2, and currents I_1, , I_2. V_1, V_2 are considered known and independent of each other, while the dependency of the rest can be defined by the admittance, that is:

$$\begin{bmatrix} I_1 \\ I_2 \end{bmatrix} = \begin{bmatrix} Y_{11} & Y_{12} \\ Y_{21} & Y_{22} \end{bmatrix} \begin{bmatrix} V_1 \\ V_2 \end{bmatrix} . \quad (1)$$

The matrix parameters Y_{11} and Y_{22} represent the ports' self-admittance, i.e. dependence of each port's current on its own voltage, while Y_{12} and Y_{21} give the cross-admittances. A matrix where $Y_{12} = G$, $Y_{21} = -G$ and $Y_{11} = Y_{22} = 0$, describes an ideal *gyrator* element [46,48].

A. Two-Port Admittance Modelling of a Switched-Resonator Network

Consider a generalized switched-resonant converter, illustrated in Fig. 3 with average port voltages V_1, V_2, and a switch assembly that applies N combinations of V_1 and V_2, i.e. *states*, on the resonator (i.e., series connection of L and C). A soft-switching mechanism that is employed, assures transition between states at zero current after half-resonance period. Since the resonant behavior in each state is of a 2nd order, the converter can be analyzed in a discrete form by viewing the potential applied on the tank (resonator) during the state's interval and determining the values at the end of each state.

The tank's capacitor voltage at the end of state n, namely $V_{C,n}$, can be derived from its initial condition, $V_{C,n-1}$, and the dc voltage that is applied on the tank during the state, namely E_n (e.g. if at state n the tank is connected directly to the source V_1 then $E_n = V_1$). Assuming sufficiently high quality-factor, i.e. negligibly small losses, $V_{C,n}$ can be expressed at the half-resonance switching-point as

$$V_{C,n} \approx 2E_n - V_{C,n-1} \quad , \quad E_n = f(V_1, V_2) . \quad (2)$$

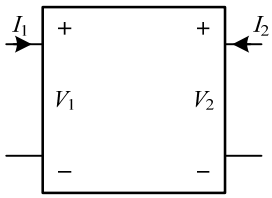

Fig. 2 Two-port

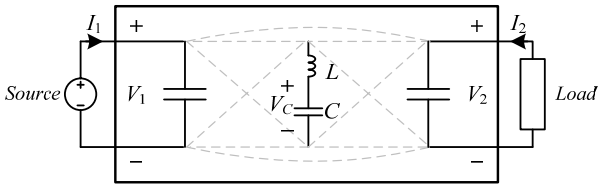

Fig. 3 A view of a switched-resonator network with dashed-lines representing possible connection alternatives to the input and output ports.

Populating the values for E_n into (2) for each of the states gives N equations with N unknowns $V_{C,1}$ to $V_{C,N}$. Assuming that all equations are independent, a unique solution exists with all the unknowns a function of V_1 and V_2, i.e. the steady-state values for $V_{C,1}$ to $V_{C,N}$ are fixed and known. It should be noted that some switching combinations may result in dependent equations which still converge to a solution when symmetrical voltages are applied on the resonator [46], that is:

This article has been accepted for publication in a future issue of this journal, but has not been fully edited. Content may change prior to final publication. Citation information: DOI 10.1109/JESTPE.2018.2878925, IEEE Journal of Emerging and Selected Topics in Power Electronics

$$\sum_{n=1}^{N} E_n \left(-1\right)^{n-1} = 0 \tag{3}$$

The average current value in each state, $I_{C,n}$, is derived from the total charge difference from the previous state, that is:

$$I_{C,n} \approx \frac{2C}{T_{state}}\left(V_{C,n} - V_{C,n-1}\right) \quad , \quad T_{state} = \pi\sqrt{LC} \tag{4}$$

where L and C are the inductance and capacitance of the resonator, respectively. Once $I_{C,n}$ is obtained for the complete sequence, I_2 can be derived by averaging all the state currents throughout the cycle in which the resonator connects to the output node. I_1 is derived in a similar manner. This yields:

$$\begin{aligned} I_1 &= F\,T_{state}\sum_{n=1}^{N} x_n I_{C,n} \quad , \quad x_n \in \{-1,0,1\} \\ I_2 &= F\,T_{state}\sum_{n=1}^{N} y_n I_{C,n} \quad , \quad y_n \in \{-1,0,1\} \end{aligned} \quad , \tag{5}$$

where F is limited by the repetition rate of the cycle, i.e. the frequency for the sum of switching states that compose one cycle $F \le F_{max} = (N\,T_{state})^{-1}$, and x_n, y_n are constants which indicate whether the tank is connected to the input and/or output at state n as well as the connection polarity. Current regulation can be obtained by modifying F with pulse-density modulation techniques [44], affecting the result of (5).

Since (2)-(5) can be rewritten as a function of V_1 , V_2, after some manipulation (5) can be expressed as a function of the admittances as:

$$I_1 = Y_{11}V_1 + Y_{12}V_2 \quad , \quad I_2 = Y_{21}V_1 + Y_{22}V_2 \ , \tag{6}$$

i.e. depends entirely on L, C and F

B. Efficiency Modelling

The efficiency of the converter can be obtained by evaluating the losses P_{loss} and the output power P_{load}, which form:

$$\eta = \left[1 + P_{loss}/P_{load}\right]^{-1} \ . \tag{7}$$

P_{loss} is obtained by summing the individual losses created in each state. Assuming no other significant losses thanks to the ZCS, the losses are due to the rms currents $I_{C,n,rms}$, through the conduction path resistance R. The total power dissipation can then be obtained using (4), with the average-to-rms ratio for a sine wave as:

$$P_{loss} = R\sum_{n=1}^{N} {I_{C,n,rms}}^2 \approx F\,T_{state} R\frac{\pi^2}{8}\sum_{n=1}^{N} {I_{C,n}}^2 \ , \tag{8}$$

where R is assumed here identical for all states to simplify the expression of (8) without loss of generality. It should be noted that for discrete as-well-as integrated design, optimizing the transistors sizes may be preferred, depending on the desired conversion ratio. Recent work which provides IC design guidelines for a GRSCC [57] presents a detailed analysis of (8) .

In a similar way to the generalization obtained in (6) for the inputs and outputs, ${I_{C,n}}^2$ can be rewritten using (2) and (4) as a general squared function of V_1, V_2, C and T_{state}. This can be expressed as

$$P_{loss} = \frac{F\,R\,C^2}{T_{state}}\left(\alpha {V_1}^2 + \beta {V_2}^2 - \gamma V_1 V_2\right) \ , \tag{9}$$

where the constants α, β, γ are weighting-factors of V_1 , V_2 based on the mode of operation.

The output power can also be directly expressed by V_1 and V_2 and the parameters of the converter's admittance (6). This yields:

$$P_{load} = -P_2 = -\left(Y_{21}V_2V_1 + Y_{22}{V_2}^2\right). \tag{10}$$

In cases where the loss contribution of Y_{22} is relatively small, and (10) can be substituted into (7) to form an efficiency expression that depends directly on the conversion ratio, A:

$$\eta = \left[1 + B\left(\alpha A^{-1} + \beta A - \gamma\right)\right]^{-1} , \ A = \frac{V_2}{V_1} \ , \tag{11}$$

where B combines the independent parameters from (9) and (10). It can be seen from (11) that as described in [36], the efficiency variation of the switched-resonator network described here depends on the conversion ratio alone.

Taking the derivative of (11) and equating to zero yields the conversion ratio in which the peak efficiency can be achieved, that is:

$$A_{optimal} = A\big|_{\max(\eta)} = \sqrt{\frac{\alpha}{\beta}} \ . \tag{12}$$

This implies that, assuming operation under ZCS and that the resonator is switched periodically after half-resonance, the location of the peak efficiency point is a weighted-function of the ports' voltages and can be adjusted by the applied voltage on the resonator, i.e. by modifying the switching sequence. This provides a new design direction and guideline for SCCs and their derivatives, as will be shown next, enabling to shift the rigid optimal target voltage by manipulating the applied voltage on the energy-transfer cell.

III. Wide-Conversion Ratio Operation Modes

The SwRC topology presented in Fig. 1 provides seven possible switching states delineated in Fig. 4 as S_A through S_G, in which the resonator may be subjected to the following potentials:

$$\begin{matrix} E_A = V_1 & E_C = -V_1 & E_E = V_1 - V_2 \\ E_B = V_2 & E_D = -V_2 & E_F = V_2 - V_1 \end{matrix} \quad E_G = 0 \tag{13}$$

Ten modes of operation are presented next to showcase the flexibility to adjust the current sourcing capabilities of the converter and to shift the peak efficiency point to target specific operating conditions. A key factor in defining a switching sequence is to assure that charge balance of the flying capacitor is maintained within a cycle. The operation modes, i.e. the voltages that are applied on the resonator per state, are chosen such that the capacitor voltage at the end of a switching sequence resumes its initial values. This condition is satisfied if a solution to (2) exists. The new operation modes of this study are defined with respect to the method in which the voltage is applied on the resonator, and compared to the originally presented a basic GRSCC with optimal conversion ratio of A =

This article has been accepted for publication in a future issue of this journal, but has not been fully edited. Content may change prior to final publication. Citation information: DOI 10.1109/JESTPE.2018.2878925, IEEE Journal of Emerging and Selected Topics in Power Electronics

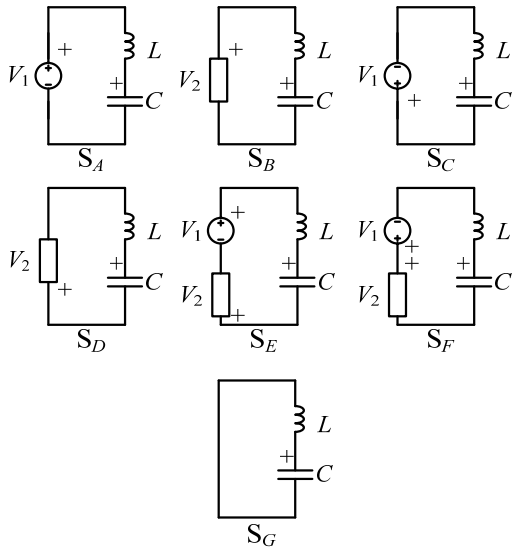

Fig. 4 Possible connection states for the converter presented in Fig. 1. Active switches for the various states. . S_A: Q_{1a}, Q_{3b}; S_B: Q_{2a}, Q_{3b}; S_C: Q_{3a}, Q_{1b}; S_D: Q_{3a}, Q_{2b}; S_E: Q_{1a}, Q_{2b}; S_F: Q_{2a}, Q_{1b}; S_G: Q_{2a}, Q_{2b}

1 [36] as a benchmark. Typical waveforms of the operation modes are depicted in Fig. 5, and the calculated conversion and efficiency characteristics of the operation modes are summarized in Table I.

TABLE I: VARIANCES BETWEEN OPERATION MODES

Mode	*a*	*b*	*c*	*d*	*e*	*f*	*g*	*h*	*i*	*j*
5-state operation		✓		✓		✓		✓		
Bridge			✓	✓			✓	✓		✓
Semi-complementary (inverted output)					✓	✓	✓	✓		
Complementary (symm. operation)									✓	✓

It should be noted that per the selection of target range of conversion ratio and output power, the generalized converter of Fig. 1 can be simplified for the number of operating switches and controller [36]. It should be further noted that in case the generalized converter is realized, then it is possible (demonstrated in the experimental section) to continuously and smoothly shift between the various operation modes as well as generate any desired combination between them. This is enabled since charge-balance of the resonator (and its flying capacitor) is guaranteed per mode and as a result, cycle-by-cycle transition between the modes is allowed without any deviation of the variables or delay.

TABLE II: PERFORMANCE CHARACTERISTICS

Mode	***a***	***b***	***c***	***d***	***e***
Sequence	S_A, S_B, S_G	S_A, S_B, S_A, S_B, S_G	S_E, S_B, S_G	S_E, S_B, S_E, S_B, S_G	S_A, S_B, S_D
F_{max}	$\left(3\pi\sqrt{LC}\right)^{-1}$	$\left(5\pi\sqrt{LC}\right)^{-1}$	$\left(3\pi\sqrt{LC}\right)^{-1}$	$\left(5\pi\sqrt{LC}\right)^{-1}$	$\left(3\pi\sqrt{LC}\right)^{-1}$
$V_{C,n}$	$\begin{cases} V_{C,1}\approx V_1+V_2 \\ V_{C,2}\approx V_2-V_1 \\ V_{C,3}\approx V_1-V_2 \end{cases}$	$\begin{cases} V_{C,1}\approx 2V_2 \\ V_{C,2}\approx 0 \\ V_{C,3}\approx 2V_1 \\ V_{C,4}\approx 2V_2-2V_1 \\ V_{C,5}\approx 2V_1-2V_2 \end{cases}$	$\begin{cases} V_{C,1}\approx V_1 \\ V_{C,2}\approx 2V_2-V_1 \\ V_{C,3}\approx V_1-2V_2 \end{cases}$	$\begin{cases} V_{C,1}\approx 2V_2 \\ V_{C,2}\approx 0 \\ V_{C,3}\approx 2V_1-2V_2 \\ V_{C,4}\approx 4V_2-2V_1 \\ V_{C,5}\approx 2V_1-4V_2 \end{cases}$	$\begin{cases} V_{C,1}\approx V_1+2V_2 \\ V_{C,2}\approx -V_1 \\ V_{C,3}\approx V_1-2V_2 \end{cases}$
$Y_{m,n}$	$\begin{bmatrix} 0 & 2FC \\ -2FC & 0 \end{bmatrix}$	$\begin{bmatrix} 0 & 4FC \\ -4FC & 0 \end{bmatrix}$	$\begin{bmatrix} 0 & 2FC \\ -2FC & 0 \end{bmatrix}$	$\begin{bmatrix} 0 & 4FC \\ -4FC & 0 \end{bmatrix}$	$\begin{bmatrix} 0 & 4FC \\ -4FC & 0 \end{bmatrix}$
η	$\left[1+\frac{\pi R}{2\sqrt{L/C}}\left(A^{-1}+A-1\right)\right]^{-1}$	$\left[1+\frac{\pi R}{4\sqrt{L/C}}\left(2A^{-1}+5A-2\right)\right]^{-1}$	$\left[1+\frac{\pi R}{2\sqrt{L/C}}\left(A^{-1}+3A-3\right)\right]^{-1}$	$\left[1+\frac{\pi R}{4\sqrt{L/C}}\left(2A^{-1}+9A-6\right)\right]^{-1}$	$\left[1+\frac{\pi R}{4\sqrt{L/C}}\left(A^{-1}+3A\right)\right]^{-1}$
$A_{opt.}$	1	0.63	0.58	0.47	0.58

PERFORMANCE CHARACTERISTICS (CONTINUED)

Mode	***f***	***g***	***h***	***i***	***j***
Sequence	S_A, S_B, S_A, S_B, S_D	S_E, S_B, S_D	S_E, S_B, S_E, S_B, S_D	S_A, S_B, S_C, S_D	S_E, S_B, S_F, S_D
F_{max}	$\left(5\pi\sqrt{LC}\right)^{-1}$	$\left(3\pi\sqrt{LC}\right)^{-1}$	$\left(5\pi\sqrt{LC}\right)^{-1}$	$\left(4\pi\sqrt{LC}\right)^{-1}$	$\left(4\pi\sqrt{LC}\right)^{-1}$
$V_{C,n}$	$\begin{cases} V_{C,1}\approx 3V_2 \\ V_{C,2}\approx -V_2 \\ V_{C,3}\approx 2V_1+V_2 \\ V_{C,4}\approx V_2-2V_1 \\ V_{C,5}\approx 2V_1-3V_2 \end{cases}$	$\begin{cases} V_{C,1}\approx V_1+V_2 \\ V_{C,2}\approx V_2-V_1 \\ V_{C,3}\approx V_1-3V_2 \end{cases}$	$\begin{cases} V_{C,1}\approx 3V_2 \\ V_{C,2}\approx -V_2 \\ V_{C,3}\approx 2V_1-V_2 \\ V_{C,4}\approx 3V_2-2V_1 \\ V_{C,5}\approx 2V_1-5V_2 \end{cases}$	$\begin{cases} V_{C,1}\approx V_1+V_2 \\ V_{C,2}\approx V_2-V_1 \\ V_{C,3}\approx -\left(V_1+V_2\right) \\ V_{C,4}\approx V_1-V_2 \end{cases}$	$\begin{cases} V_{C,1}\approx V_1 \\ V_{C,2}\approx 2V_2-V_1 \\ V_{C,3}\approx -V_1 \\ V_{C,4}\approx V_1-2V_2 \end{cases}$
$Y_{m,n}$	$\begin{bmatrix} 0 & 8FC \\ -8FC & 0 \end{bmatrix}$	$\begin{bmatrix} 0 & 4FC \\ -4FC & 0 \end{bmatrix}$	$\begin{bmatrix} 0 & 8FC \\ -8FC & 0 \end{bmatrix}$	$\begin{bmatrix} 0 & 4FC \\ -4FC & 0 \end{bmatrix}$	$\begin{bmatrix} 0 & 4FC \\ -4FC & 0 \end{bmatrix}$
η	$\left[1+\frac{\pi R}{8\sqrt{L/C}}\left(5A^{-1}+9A-6\right)\right]^{-1}$	$\left[1+\frac{\pi R}{4\sqrt{L/C}}\left(A^{-1}+4A-2\right)\right]^{-1}$	$\left[1+\frac{\pi R}{4\sqrt{L/C}}\left(A^{-1}+10A-2\right)\right]^{-1}$	$\left[1+\frac{\pi R}{4\sqrt{L/C}}\left(A^{-1}+A\right)\right]^{-1}$	$\left[1+\frac{\pi R}{4\sqrt{L/C}}\left(A^{-1}+2A-2\right)\right]^{-1}$
A_{opimal}	0.74	0.5	0.58	1	0.71

This article has been accepted for publication in a future issue of this journal, but has not been fully edited. Content may change prior to final publication. Citation information: DOI 10.1109/JESTPE.2018.2878925, IEEE Journal of Emerging and Selected Topics in Power Electronics

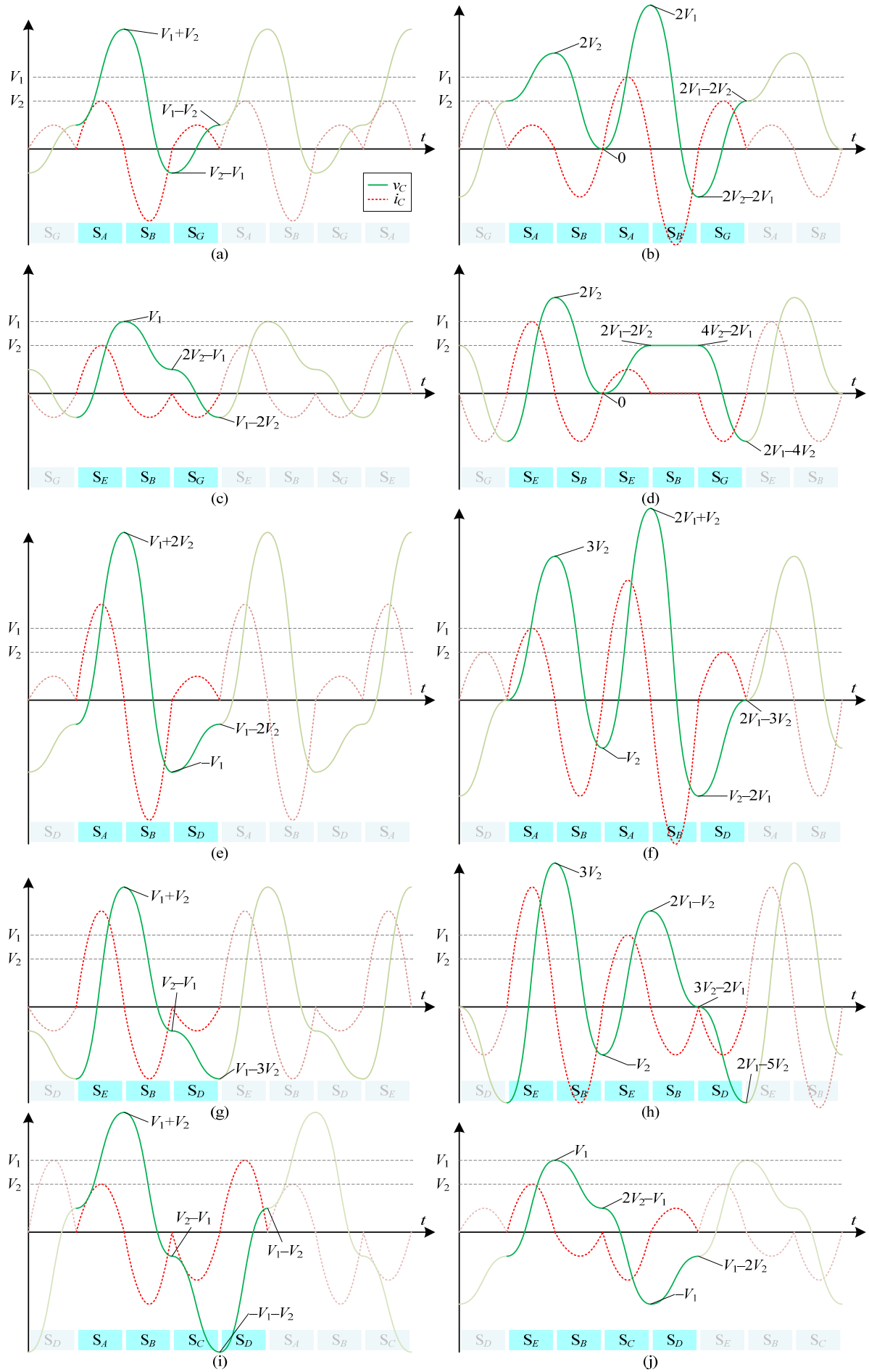

Fig. 5 Exemplary waveforms of the presented family for a case that $V_1 = 1.5V_2$ for all modes: (a)-(j)

This article has been accepted for publication in a future issue of this journal, but has not been fully edited. Content may change prior to final publication. Citation information: DOI 10.1109/JESTPE.2018.2878925, IEEE Journal of Emerging and Selected Topics in Power Electronics

A benchmark operation mode is the case of a basic GRSCC configuration. In this mode (sequence: S_A, S_B, S_G), namely *mode (a)* was originally implemented in [36] by a three-switch configuration. The resonator connects to the input through configuration S_A (Fig. 4) to charge, then by S_B to the output voltage and discharges. In order to achieve charge balance, the resonator is then short-circuited through S_G to circulate excess charge.

Five-state operation – In a variation from mode (a), the input and output potentials are applied twice on the resonator before a charge balance state is commenced. The operation is: charge the resonator by S_A, discharge by S_B, charge and discharge again by S_A and S_B, and then end the sequence by S_G to circulate excess charge. By effectively reducing circulation time, the overall time allocated for charge and discharge is increased. This intuitively implies (and validated later in this subsection) that higher current can be outputted since a larger portion of the cycle is devoted to process energy compared to the portion dedicated to balance the charge (in which energy is recycled but not transferred). This method of operation is denoted as *mode (b)*, and used as the basis for more modes discussed next.

Bridge variation [36,57] – An alternative method from mode (a) to process energy by the converter is to subject the resonator to the voltage difference between the input and the output [i.e. S_E, see Fig. 4], providing a lower voltage potential than in the unit mode. The charge state S_E is, like in mode (a), followed by S_B that applies the output voltage on the resonator and charge balance is achieved by a short-circuit [S_G, Fig. 4]. This provides the operation sequence for *mode (c)*, and the basis for more modes, e.g. the bridge variation can also be used for five-state operation, presented here as *mode (d)*.

Semi-complementary operation – In another variation of the switching sequence, charge balance can be facilitated through a different switching state, replacing the resonant short-circuit (S_G) by a complementary connection to V_2, providing new semi-complementary operation. In the charge state S_A the resonator is subjected to V_1. Then, by applying S_B, the network connects to V_2 and charge is transferred to the output. Charge balance is achieved in these modes through state S_D which applies a negative voltage ($-V_2$). This variation is presented here as *mode (e)*, however it can be combined with any of the variations mentioned earlier, forming *modes (f)-(h)*, as summarized in Table I.

Complementary operation – This variation provides symmetric operation of the converter, as positive voltages are applied on the resonator, followed by their negative counterparts to achieve charge balance. By initiating S_A, the resonator is subjected to V_1 and charges, then it is subjected to V_2 to discharge by applying state S_B. To maintain charge balance the resonator is then inversely charged by S_C that subjects it to the negative potential $-V_1$, and then discharged by S_D which applies the negative voltage ($-V_2$). Complementary operation can be applied as described here to form *mode (i)*, or combined with the bridge variation to form *mode (j)*.

The complete sequences and performance parameters for the ten possible modes formed by combining the above variations are summarized in Table II, with characteristic resonator waveforms for each mode illustrated in Fig. 5. Comparison between the modes of operation reveals several differences in the properties of the new family. It can be observed that although identical conditions are applied in terms of the ports' voltages and components values, the resultant admittance matrices of the new modes are doubled, and sometimes quadrupled in value when compared to the benchmark mode This directly translates to increased current sourcing capability of the converter. Using the five-state operation in mode (b) increases the power output by 1.2, as admittance is doubled but the effective frequency is lowered by 0.6. The semi-complementary mode (e) is capable of outputting twice the power than mode (a) for the same conditions (frequency and R, L, C values). Combining the two to form a five-state semi-complementary mode (f) increases the power output capability by a factor of 2.4. The complementary mode's (i) output power capability is higher than the benchmark by a factor of 1.5, as admittance is doubled and frequency is lower by 0.75.

Seemingly, minor difference on the power delivery capabilities is observed between the unity and bridge assembly variations for modes [(c),(d),(g),(h),(j)]. However, a major difference is found in the efficiency as a function of the conversion ratio A. As an example, when comparing the waveforms of modes (a) and (c), it can be seen that the bridge variation induces significantly lower circulating current on the converter for a gain of A=0.75, implying difference in the efficiency characteristics when using the bridge variation.

The efficiency expressions from Table II have been plotted for better view and are presented in Fig. 6 for all modes. In Fig. 6(a-c) a case in which equal resonator parameters are used for all modes is depicted. It can be seen that for the majority of conversion ratios the converter is most efficient when using the complementary mode (j), with peak efficiency at $A = 0.71$. Bridge variations do not change the power delivery capabilities but have a major impact on the efficiency: both in the peak location and value. However, it can be seen that five-state sequences for example, increase the power output at the cost of a narrower applicable efficiency range. This can be explained by major increase in rms curents due to the large mismatch between the port voltages, as can be easily observed in the example of Fig. 5(f), which demonstrates high divergence in the current prior to the balance state (S_D).

Since the power delivery capabilities differ between the modes, an alternative comparison between modes has been performed by normalizing the operation to the same power delivery level. In Fig. 6(d-f), the resonator's parameters are adapted such that the total admittance matrix values (considering the maximum frequency) are the same for all modes, i.e. for the same power delivery capability. It can be seen that all modes are distinctively more efficient than the benchmark configuration. A highlighted example is that for the same power delivery capability, mode (j) provides higher efficiency of at least 7% for any gain. On selected range of conversion ratios, such as A=0.3, the semi-complementary mode (d) allows for higher efficiency than (j).

This article has been accepted for publication in a future issue of this journal, but has not been fully edited. Content may change prior to final publication. Citation information: DOI 10.1109/JESTPE.2018.2878925, IEEE Journal of Emerging and Selected Topics in Power Electronics

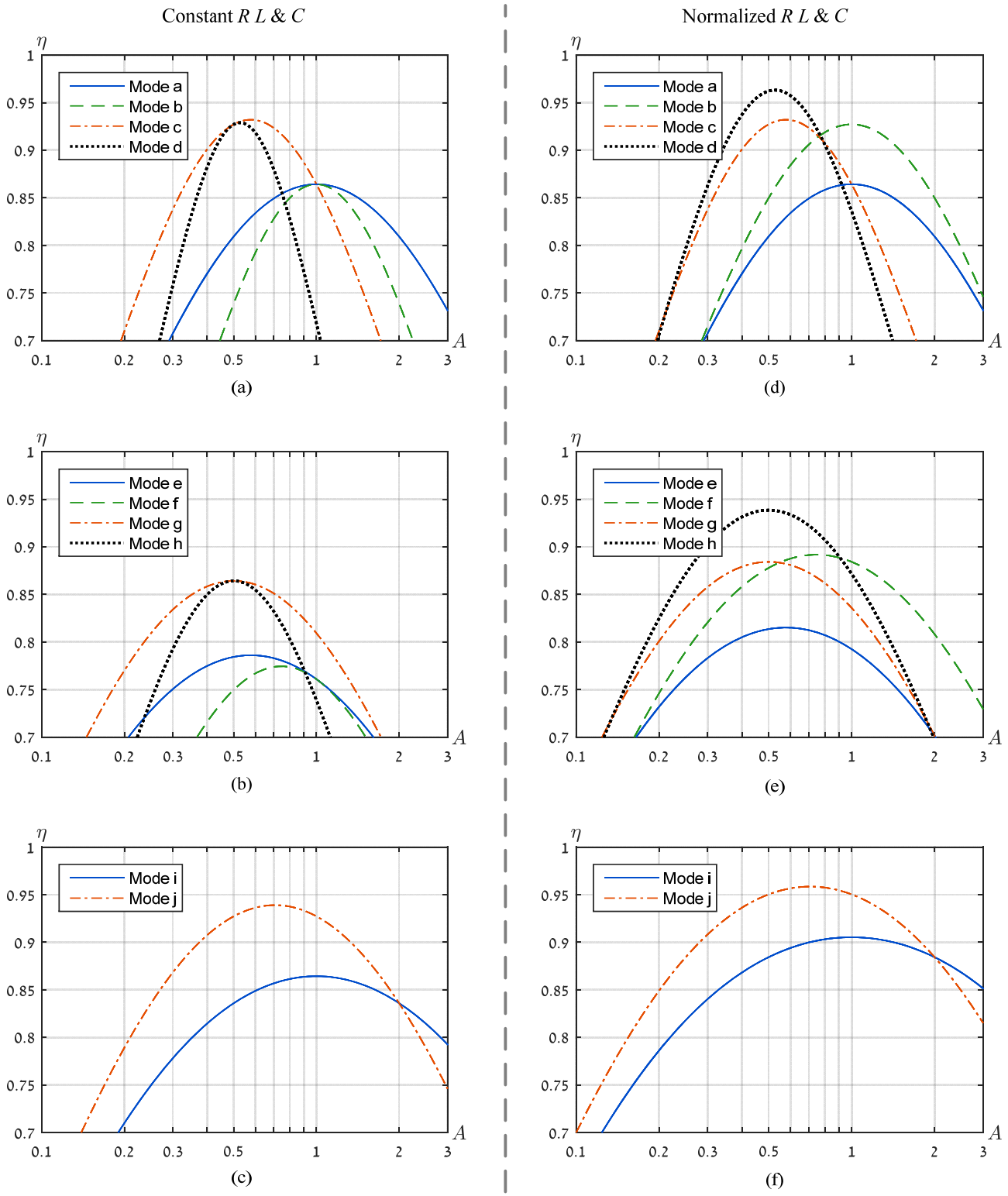

Fig. 6 Theoretically calculated efficiency plots of the presented converter as a function of conversion ratio for the ten presented operating modes when: Left (a)-(c) R,L,C are the same in all topologies providing a quality factor of $Q = 10$; (d)-(f) Resonator impedance is equal for all modes.

This article has been accepted for publication in a future issue of this journal, but has not been fully edited. Content may change prior to final publication. Citation information: DOI 10.1109/JESTPE.2018.2878925, IEEE Journal of Emerging and Selected Topics in Power Electronics

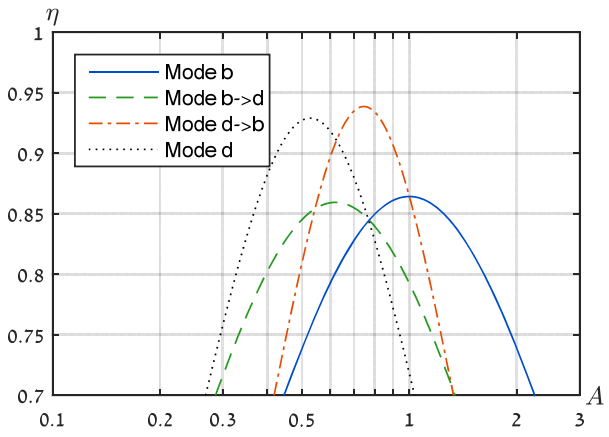

Fig. 7 Theoretically calculated efficiency plots of the presented converter as a function of conversion ratio comparing interleaved modes to non-interleaved.

Further flexibility on the power delivery capabilities can be obtained by combining modes of operation. For instance, mixture of modes b and d can result in a sequences such as S_A, S_B, S_E, S_B, S_G (namely mode b-d) or S_E, S_B, S_A, S_B, S_G (namely mode d-b). Mode d-b has a reduced output admittance of $Y_{21}=2FC$, while mode b-d as an increased output admittance of $Y_{21}=4FC$. The efficiency curves of these modes are shown non normalized in Fig. 7.

IV. Application

In similar way to the GRSCC topology [36] and as described next, some switches of the SwRC family can be implemented either by simple, single, transistor or by four-quadrant switches (reverse-blocking) such as a back-to-back configuration. For a case that a step-down is desired, then Q_{1a} and Q_{1b} need to be implemented as four-quadrant devices for proper operation. In this case the *resonator* is inherently clamped to V_1 without losing operability when the *capacitor* charges to higher voltage. In this case, the maximum voltage stress on switches $Q_{1a,b}$ and $Q_{3a,b}$ is the source value V_1.

An additional implementation variation is with Q_{2a} and Q_{2b} as four-quadrant switches. This provides higher flexibility of the converter, allowing step-up and step-down conversion. This comes at the cost of higher component count and losing the inherent resonator-clamp.

The presented SwRC family extends the GRSCC family and provides true voltage regulation capabilities with the added value of immediate transient-response capabilities, previously shown in [36,44]. These unique features allow the high power-density property of the SCC family to be utilized in a variety of new applications such as envelope-tracking [45], voltage-regulation in high-transient applications [58,59]. Furthermore, recent studies which have presented high power-density regulation schemes using SCC technology [32,33] still require a post-regulation at point-of-load. Table III provides a topology comparison for post-regulation schemes used today, compared to the proposed family. As will be demonstrated in the experimental section, the presented family facilitates efficient post-regulation using SCC technology.

TABLE III: Key Attributes Comparison Between Topologies

	SCC	***RSCC***	***Buck***	***GRSCC***	***SwRC***
Efficiency characteristics	Singular	Singular	Wide	Narrow	Adjustable
Soft-switching capability	×	✓	×	✓	✓
Scalability	Limited by switching-loss	✓	Limited by switching-loss & large inductance	✓	✓
Component stress	Clamped to source voltages	Clamped to source voltages	Clamped to source voltages	Clamped to source voltages	Clamped to source voltages

V. Experimental Verification

To demonstrate the operation of the various modes of the SwRC and to validate the theoretical analysis, a low output-voltage prototype was built and tested $V_1=5$V to $V_2=1.2$V, with a photograph of the experimental board in Fig. 8. The resonator's parameters were $C=220$nF, $L\approx 40$nH ($T_{state}=300$ns), the MOSFETs used where Siliconix SIA436EDJ, driven by MAX17601 drivers. The prototype was tested for three most promising modes for this conversion gain: modes (b), (g), (j). Experimental waveforms of the resonator's current and the capacitor's voltage operating in steady-state are shown in Fig. 9; the differences between the modes are apparent. The output power of the bridge-GRSCC was measured 2.75W, for the complementary mode 3.9W and for the semi-complementary 5.1W. These results are in excellent agreement with the theoretical prediction from Table I and exhibit a unique capability of efficiently regulating a low output voltage, which needed for applications such as point-of-load regulation – a weak-point for conventional SCCs.

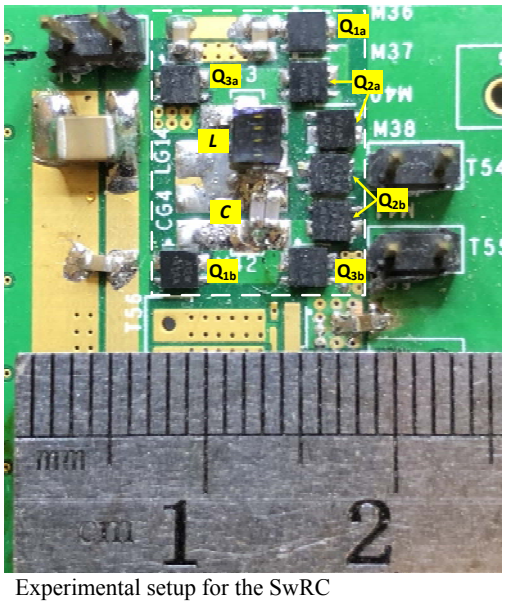

Fig. 8 Experimental setup for the SwRC

This article has been accepted for publication in a future issue of this journal, but has not been fully edited. Content may change prior to final publication. Citation information: DOI 10.1109/JESTPE.2018.2878925, IEEE Journal of Emerging and Selected Topics in Power Electronics

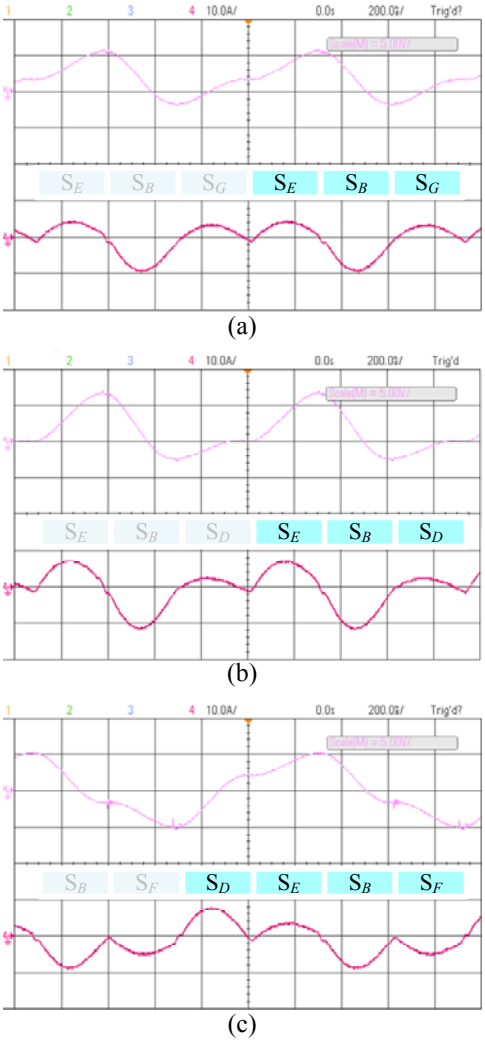

Fig. 9 Experimental waveforms of the presented converter for the following modes showing vC at the top and iC at the bottom of each screenshot: (a) bridge-GRSCC; (b) semi-complementary; (c) complementary.

Fig. 10(a) shows the efficiency as a function of the conversion ratio comparing modes *b*, *g* and *j*. These measurements were carried out using an electronic load that was programmed to sweep V_2. The cycle frequency of the converters was set to maximum - F_{max}, i.e. maximizing the power output capability at each of the modes. As can be seen, a very good agreement is obtained with the theoretical curves of Fig. 6. Also demonstrated is the different conversion ratio for the peak efficiency at each of the modes. Fig. 10(b) shows an experimental efficiency plot demonstrating the hybrid combinations of modes b and d as in Fig. 7, validating the flexibility in choice of switching options to obtain different converter properties in terms of efficiency.

To further illustrate the dynamic properties of the converter, a 2:1 switched-resonant system was tested, which includes three dedicated switches associated with states $\{S_A, S_B, S_G\}$ providing three voltages $\{V_1, V_2, 0\}$. The system is programmed to alternate between the two basic modes: mode *a* and mode *b*. The former has been demonstrated to be generally more efficient (see Fig. 6a) while the latter provides increased current delivery capabilities. Alternating between these two modes can be useful when high efficiency is desired in normal operation modes, while trading for power when current boost is needed. The basic data of the experimental system are as follows: $V_1 = 10\text{V}$, $V_2 = 5\text{V}$, $C = 33\text{nF}$, $L \approx 75\text{nH}$, $t_{on} = 160\text{ns}$; the MOSFETs used where Siliconix SIA466EDJ, driven by MAX17601 drivers.

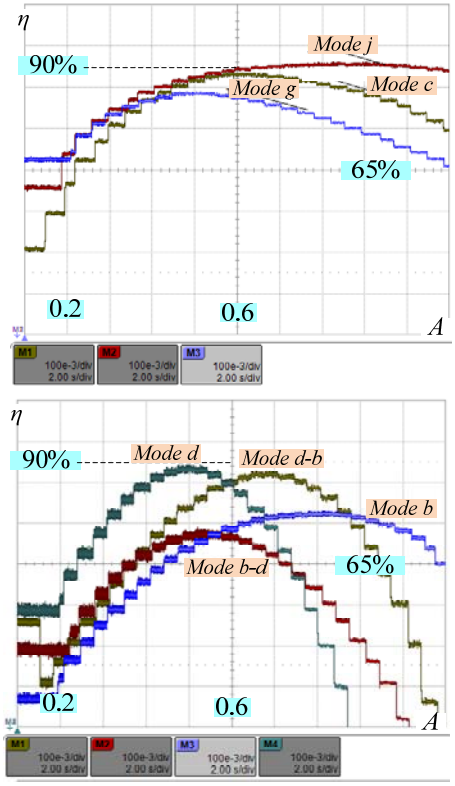

Fig. 10 Experimental efficiency sweep as a function of output voltage gain. Vertical: 10%/Div. ; Horiz.: 0.1/Div. (a) comparison between modes c, g, and j; (b) comparison of modes d, b, and their derivatives, mode d b-d and d-b.

The experimental results demonstrated in Fig. 11 show a fast, one cycle response, of the switched-resonant converter upon a change from one mode to the other. The ratio of the experimental average currents of V_1 and V_2 has been found to be $1.45\text{A} / 1.65\text{A} = 0.878$ while the model prediction is $(1/2)\,(3/5) = 0.833$. The discrepancy is explained by the fact that the efficiencies for the two cases are different due to the differences in the rms currents. The efficiency for the 3 switching states case is measured to be 80% while the efficiency for the 5 states is 77%. Correction of the experimental currents ratio by the efficiencies ratio $\{(0.878\,(77 / 80) = 0.845\}$ shows very good agreement of the theoretically calculated values and the measured results.

VI. Conclusion

A new switched-resonant converter with many possible modes of operation has been presented and demonstrated efficiency characteristics that exhibit a broad peak over an extended voltage gain-range. The capability to shape the efficiency characteristics of the converter has been demonstrated through ten modes of operation. This attribute, *resided thus far only in multi-target voltage converters that employ several energy-transfer cells*, realized in this work by a single energy transfer cell.

This article has been accepted for publication in a future issue of this journal, but has not been fully edited. Content may change prior to final publication. Citation information: DOI 10.1109/JESTPE.2018.2878925, IEEE Journal of Emerging and Selected Topics in Power Electronics

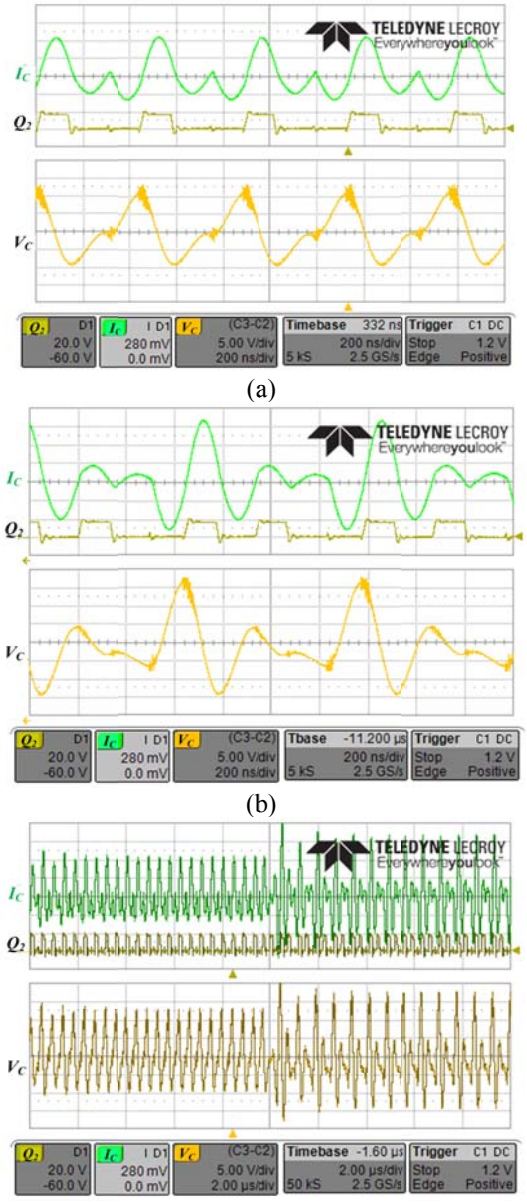

Fig. 11 Experimental results of transition from mode *a* to mode *b*: (a) mode *a*; (b) mode *b*; (c) transition. The upper trace is converter's current (relative scale) and the lower trace is the capacitor's voltage (5V/Div.).

A generalized procedure to describe switched-resonant or resonant-type switched-capacitor converters with multiple operation-modes as two-port networks has been described to evaluate and quantify the characteristics of such converters in various conditions. Three operation modes have been demonstrated and evaluated both theoretically end experimentally, providing different power-sourcing and efficiency capabilities. Experimental results demonstrate an increase of over 10% in efficiency at high conversion ratios compared the previously presented Bridge-GRSCC.

Combining the benefits of the relatively simple converter design and the need for a single energy-transfer cell to allow continuous high-efficiency conversion ratios, the GRSCC-based voltage regulator can be considered as an attractive candidate for voltage regulation applications that require high response rate. Furthermore, the possibility of multiple operation modes allows flexibility in the converter design and further size reduction of the resonator.

REFERENCES

[1] M. S. Makowski and D. Maksimovic, "Performance limits of switched-capacitor dc-dc converters," IEEE Power Electronics Specialists Conference, vol. 2, pp. 1215-1221, 1995.

[2] M. Budaes and L. Goras, "Burst mode switching mechanism for an inductorless dc-dc converter," *CAS International Semiconductor Conference*, vol. 2, pp.463-466, 2007.

[3] M. D. Seeman and S. R. Sanders, "Analysis and optimization of switched capacitor dc-dc converters," *IEEE Transactions on Power Electronics,* vol. 23, no. 2, pp. 841-851, 2008.

[4] S. Ben-Yaakov and M. Evzelman, "Generic and unified model of switched capacitor converters," *IEEE Energy Conversion Congress and Exposition,* pp. 3501-3508, 2009.

[5] J. M. Henry and J. W. Kimball, "Practical performance analysis of complex switched-capacitor converters," *IEEE Transactions on Power Electronics*, vol. 26, no. 1, pp. 127-136, 2011.

[6] S. Ben-Yaakov, "On the influence of switch resistances on switched capacitor converters losses," *IEEE Transactions on Industrial Electronics, Letters*, vol. 59, no. 1, pp. 638-640, 2012.

[7] J. M. Henry and J. W. Kimball, "Switched-capacitor converter state model generator," *IEEE Transactions on Power Electronics*, vol.27, no.5, pp.2415-2425, 2012.

[8] P. K. Peter and V. Agarwal, "On the input resistance of a reconfigurable switched capacitor dc–dc converter-based maximum power point tracker of a photovoltaic source," *IEEE Transactions on Power Electronics*, vol. 27, no. 12, pp. 4880-4893, 2012.

[9] M. Evzelman and S. Ben-Yaakov, "Average-current based conduction losses model of switched capacitor converters," *IEEE Transactions on Power Electronics,* vol. 28, no. 7, pp. 3341-3352, 2013.

[10] B. Wu, L. Wang, L. Yang, K. Smedley, and S. Singer, "comparative analysis of steady-state models for switched capacitor converter," *IEEE Transactions on Power Electronics*, *Early Access,* vol. PP, no. 99, pp. 1-1, 2016.

[11] H. S. H. Chung, "Development of DC/DC regulators based on switched-capacitor circuits," *IEEE International Symposium on Circuits and Systems,* pp. 210-213 vol. 5, 1999.

[12] M. Evzelman and R. Zane, "Burst mode control and switched-capacitor converters losses," *IEEE Applied Power Electronics Conference and Exposition,* pp. 1603-1607, 2016.

[13] S. Ben-Yaakov and A. Kushnerov, "Algebraic foundation of self adjusting switched capacitors converters," *IEEE Energy Conversion Congress and Exposition,* pp. 1582-1589, 2009.

[14] R. C. N. Pilawa-Podgurski, D. M. Giuliano, and D. J. Perreault, "Merged two-stage power converter architecture with soft charging switched-capacitor energy transfer," *IEEE Power Electronics Specialists Conference*, pp. 4008-4015, 2008.

[15] S. Lim, J. Ranson, D. M. Otten, and D. J. Perreault, "Two-stage power conversion architecture for an LED driver circuit," *IEEE Applied Power Electronics Conference and Exposition,* pp. 854-861, 2013.

[16] Y. Beck and S. Singer, "Capacitive transposed series-parallel topology with fine tuning capabilities," *IEEE Transactions Circuits Systems I, Regular Papers*, vol. 58, no. 1, pp. 51-61, 2011.

[17] A. Kushnerov and S. Ben-Yaakov, "Unified algebraic synthesis of generalized fibonacci switched capacitor converters," *IEEE Energy Conversion Congress and Exposition,* pp. 774-778, 2012.

[18] Y. Beck, S. Singer, and L. M. Salamero, "Modular realization of capacitive converters based on general transposed series-parallel and derived topologies," *IEEE Transactions Industrial Electronics*, vol. 61, no. 3, pp. 1622-1631, 2014.

[19] L. G. Salem and P. P. Mercier, "A recursive switched-capacitor dc-dc converter achieving 2^{N-1} ratios with high efficiency over a

wide output voltage range," *IEEE Journal of Solid-State Circuits*, vol. 49, no. 12, pp. 2773-2787, 2014.

[20] E. Hamo, A. Cervera, and M.M. Peretz, "Multiple conversion ratio resonant switched-capacitor converter with active zero current detection," *IEEE Transactions on Power Electronics*, vol. 30, no. 4, 2073-2083, 2015.

[21] Y.-S. Lee, Y.-Y. Chiu, and M.-W. Cheng, "ZCS switched-capacitor bi-directional quasi-resonant converters," *IEEE International Conference on Power Electronics and Drive Systems,* pp. 866-871, 2005.

[22] Y.-S. Lee and Y.-P. Ko, "Switched-capacitor bi-directional converter performance comparison with and without quasi-resonant zero-current switching," *IET Power Electronics*, vol. 3, no. 2, pp. 269-278, 2010.

[23] M. Shoyama, T. Naka, and T. Ninomiya, "Resonant switched-capacitor converter with high efficiency," *IEEE Power Electronics Specialists Conference,* vol. 5, pp. 3780-3786, 2004.

[24] Y. P. B. Yeung, K. W. E. Cheng, S. L. Ho, K. K. Law, and D. Sutanto, "Unified analysis of switched-capacitor resonant converters," *IEEE Transactions on Industrial Electronics*, vol. 51, no. 4, pp. 864-873, 2004.

[25] A. Ioinovici, H. S. H. Chung, M. S. Makowski, and C. K. Tse, "Comments on 'Unified analysis of switched-capacitor resonant converters'," *IEEE Transactions on Industrial Electronics*, vol. 54, no. 1, pp. 684-685, 2007.

[26] O. Keiser, P. K. Steimer, and J. W. Kolar, "High power resonant switched-capacitor step-down converter," *IEEE Power Electronics Specialists Conference,* pp. 2772-2777, 2008.

[27] D. Cao and F. Z. Peng, "Multiphase multilevel modular dc–dc converter for high-current high-gain teg application," *IEEE Transactions on Industry Applications*, vol. 47, no. 3, pp. 1400-1408, 2011.

[28] D. Cao and F. Z. Peng, "Zero-current-switching multilevel modular switched-capacitor dc–dc converter," *IEEE Transactions on Industry Applications*, vol. 46, no. 6, pp. 2536-2544, 2010.

[29] D. Cao, S. Jiang, and F. Z. Peng, "Optimal design of multilevel modular switched-capacitor dc-dc converter," *IEEE Energy Conversion Congress and Exposition*, pp. 537-544, 2011.

[30] K. Kesarwani, R. Sangwan, and J. T. Stauth, "Resonant-Switched Capacitor Converters for Chip-Scale Power Delivery: Design and Implementation," in *IEEE Transactions on Power Electronics*, vol. 30, no. 12, pp. 6966-6977, Dec. 2015.

[31] C. Schaef, K. Kesarwani, and J. T. Stauth, "20.2 A variable-conversion-ratio 3-phase resonant switched capacitor converter with 85% efficiency at 0.91W/mm^2 using 1.1nH PCB-trace inductors," *2015 IEEE International Solid-State Circuits Conference - (ISSCC) Digest of Technical Papers*, San Francisco, CA, 2015, pp. 1-3.

[32] Z. Ye, Y. Lei, and R.C.N. Pilawa-Podgurski, "A resonant switched capacitor based 4-to-1 bus converter achieving 2180 W/in^3 power density and 98.9% peak efficiency," *Applied Power Electronics Conference and Exposition*, pp. 121-126, 2018.

[33] S. Jiang, C. Nan, X. Li, C. Chung, and M. Yazdani, "Switched tank converters," *Applied Power Electronics Conference and Exposition (APEC)*, pp. 81-90, 2018.

[34] M. D. Seeman, V. W. Ng, H. P. Le, M. John, E. Alon, and S. R. Sanders, "A comparative analysis of switched-capacitor and inductor-based dc-dc conversion technologies," *IEEE Workshop on Control and Modeling for Power Electronics*, pp. 1-7, 2010.

[35] Y. Lei and R. C. N. Pilawa-Podgurski, "A General Method for Analyzing Resonant and Soft-Charging Operation of Switched-Capacitor Converters," *IEEE Transactions on Power Electronics*, vol. 30, no. 10, pp. 5650-5664, 2015.

[36] A. Cervera, M. Evzelman, M. M. Peretz, and S. Ben-Yaakov, "A high efficiency resonant switched capacitor converter with continuous conversion ratio," *IEEE Transactions on Power Electronics,* vol. 30, no. 3, 1373-1382, 2015.

[37] R. Beiranvand, "Analysis of a switched-capacitor converter above its resonant frequency to overcome voltage regulation issue of resonant SCCs," *IEEE Transactions on Industrial Electronics*, vol. 63, no.9, pp. 5315-5325, 2016.

[38] D. Qiu and B. Zhang, "Analysis of step-down resonant switched capacitor converter with sneak circuit state," *IEEE Power Electronics Specialists Conference,* pp. 1-5, 2006.

[39] K. Sano and H. Fujita, "A resonant switched-capacitor converter for voltage balancing of series-connected capacitors," *International Conference on Power Electronics and Drive Systems*, pp. 683-688, 2009.

[40] K. Sano and H. Fujita, "Performance of a high-efficiency switched-capacitor-based resonant converter with phase-shift control," *IEEE Transactions on Power Electronics*, vol. 26, no. 2, pp. 344-354, 2011.

[41] K.-H. Liu, R. Oruganti, and F. C. Lee, "Resonant switches-Topologies and characteristics," *IEEE Power Electronics Specialists Conference,* pp. 106-116, 1985.

[42] Y. Li, M. John, Y. Ramadass and S. R. Sanders, "An AC-coupled stacked dual active bridge hybrid DC-DC converter for battery-to-processor power delivery with 87.2% peak efficiency and high accuracy loadline regulation," *2018 IEEE Custom Integrated Circuits Conference (CICC)*, San Diego, CA, 2018, pp. 1-4.

[43] W. Liu, P. Assem, Y. Lei, P. K. Hanumolu and R. Pilawa-Podgurski, "10.3 A 94.2%-peak-efficiency 1.53A direct-battery-hook-up hybrid Dickson switched-capacitor DC-DC converter with wide continuous conversion ratio in 65nm CMOS," *2017 IEEE International Solid-State Circuits Conference (ISSCC)*, San Francisco, CA, 2017, pp. 182-183.

[44] M. Jabbari, "Unified analysis of switched-resonator converters," *IEEE Transactions on Power Electronics*, vol. 26, no. 5, pp. 1364-1376, 2011.

[45] S. Sharifi and M. Jabbari, "Family of single-switch quasi-resonant converters with reduced inductor size," *IET Power Electronics*, vol. 7, no. 10, pp. 2544-2554, 2014.

[46] A. Cervera and M. M. Peretz, "Resonant switched-capacitor voltage regulator with ideal transient response," *IEEE Transactions on Power Electronics,* vol. 30, no. 9, 4943-4951, 2015.

[47] A. Cervera and M. M. Peretz, "Envelope tracking power supply for volume-sensitive low-power applications based on a resonant switched-capacitor converter," *IEEE Applied Power Electronics Conference and Exposition*, pp. 2298-2303, 2016.

[48] A. Cervera, M. M. Peretz, S. Ben-Yaakov, "A Generic and Unified Global-Gyrator Model of Switched-Resonator Converters," in *IEEE Transactions on Power Electronics* , vol.PP, no.99, pp.1-1

[49] B. D. Tellegen, "The gyrator, a new electric network element," *Philips Research Laboratories, Reprinted*, vol. 3, no. 2, pp.81-101, 1948.

[50] S. Singer, "Gyrators application in power processing circuits," *IEEE Transactions on Industrial Electronics*, vol. IE-34, no. 3, pp. 313-318, 1987.

[51] G. Pillonnet, "Modeling and efficiency analysis of multiphase resonant-switched capacitive converters," *IEEE Transactions on Power Electronics*, vol. 31, no. 1, pp. 11-14, 2016.

[52] D. Shmilovitz, "Gyrator Realization Based on a Capacitive Switched Cell," in *IEEE Transactions on Circuits and Systems II: Express Briefs*, vol. 53, no. 12, pp. 1418-1422, 2006.

[53] Y.-H. Liu, S.-C. Wang and Y.-F. Luo, "Digital dimming control of CCFL drive system using pulse density modulation technique," *IEEE Region 10 Conference,* pp. 1-4, 2007.

[54] X. Zhang, Y. Pu, K. Ishida, Y. Ryu, Y. Okuma, P.-H. Chen, K. Watanabe, T. Sakurai, and M. Takamiya, "A 1-V-input switched-capacitor voltage converter with voltage-reference-free

pulse-density modulation," *IEEE Transactions on Circuits and Systems II: Express Briefs*, vol. 59, no. 6, pp. 361-365, 2012.

[55] B. B. Macy, Y. Lei, and R. C. N. Pilawa-Podgurski, "A 1.2 MHz, 25 V to 100 V GaN-based resonant Dickson switched-capacitor converter with 1011 W/in3 (61.7 kW/L) power density," in 2015 IEEE Applied Power Electronics Conference and Exposition (APEC), 2015, vol. 3, pp. 1472– 1478.

[56] Y. Li, J. Chen, M. John, R. Liou, and S. R. Sanders, "Resonant switched capacitor stacked topology enabling high DC-DC voltage conversion ratios and efficient wide range regulation," *2016 IEEE Energy Conversion Congress and Exposition (ECCE)*, Milwaukee, WI, 2016, pp. 1-7.

[57] E. Abramov, A. Cervera, and M. M. Peretz, "Optimal Design of a Voltage Regulator Based on Gyrator Switched-Resonator Converter IC," *IEEE Journal of Emerging and Selected Topics in Power Electronics*, vol. 6, no. 2, pp. 549-562, 2018.

[58] O. Kirshenboim, A. Cervera, B. Halivni, E. Abramov, and M. Peretz, "Plug-and-Play Electronic Capacitor for VRM Applications" *IEEE Applied Power Electronics Conference and Exposition*, pp. 111-117, 2016.

[59] O. Kirshenboim, A. Cervera, M. M. Peretz, "Improving loading and unloading transient response of a voltage regulator module using a load-side auxiliary gyrator circuit", *IEEE Transactions on Power Electronics*, vol. 32, no. 3, pp.1996-2007, 2017.